



## Combined Upper Limit on Standard Model Higgs Boson Production for Summer 2008

The CDF Collaboration  
URL <http://www-cdf.fnal.gov>  
(Dated: September 12, 2008)

This note describes a combination of searches for the Standard Model Higgs boson at CDF. The six major analyses combined are the  $WH \rightarrow \ell\nu b\bar{b}$  channels, the  $WH + ZH \rightarrow \cancel{E}_T + b\bar{b}$  channels, the  $ZH \rightarrow \ell^+\ell^- b\bar{b}$  channels, the  $H \rightarrow \tau^+\tau^-$  channel, the  $H \rightarrow W^+W^- \rightarrow \ell^+\nu_\ell\ell'^-\bar{\nu}_{\ell'}$  channels, and the  $WH \rightarrow WW^+W^-$  channel. The integrated luminosity for the channels varies between  $1.9 \text{ fb}^{-1}$  and  $3.0 \text{ fb}^{-1}$ . The 95% CL upper limit on  $R = \sigma_H/\sigma_{H,SM}$  is computed as a function of  $m_H$  from 100 to 200  $\text{GeV}/c^2$  in steps of  $5 \text{ GeV}/c^2$ , assuming Standard Model decay branching fractions of the Higgs boson and that the ratios of the rates for the  $WH$ ,  $ZH$ ,  $gg \rightarrow H$  and vector-boson fusion  $qq \rightarrow Hqq$  production mechanisms are those predicted by the Standard Model. The results are in good agreement with those expected in the background-only hypothesis, and the observed (expected) limits on  $R$  are 4.19 (3.56) and 1.52 (1.68) at Higgs boson masses of 115 and 160  $\text{GeV}/c^2$ , respectively.

*Preliminary Results for Summer 2008 Conferences*

A combination of the different Higgs search analysis results provides many advantages. Since the decay branching ratios of the Standard Model (SM) Higgs boson are strong functions of its mass  $m_H$ , the different search channels contribute in a complementary way to the sensitivity at different  $m_H$ . Some analyses seek the Higgs boson in the same decay mode but with different production mechanisms, and hence require separate treatments of the signals and backgrounds. Since these analyses all seek the same particle, the best results arise in combination.

A previous combination [1] has been performed using the results of the five main searches for the Standard Model Higgs boson at CDF, the  $WH \rightarrow \ell\nu b\bar{b}$  channels, the  $WH + ZH \rightarrow \cancel{E}_T + b\bar{b}$  channels, the  $ZH \rightarrow \ell^+\ell^-b\bar{b}$  channels, the  $H \rightarrow \tau^+\tau^-$  channel, and the  $H \rightarrow W^+W^- \rightarrow \ell^+\nu_\ell\ell^-\bar{\nu}_\ell$  channels. This note presents an update of the combination, using newly released results for all of the above channels, except the  $H \rightarrow \tau^+\tau^-$  channel [2], which remains stable. The  $WH \rightarrow WW^+W^-$  channel has been newly added for this combination. The analyses include additional data up to  $3 \text{ fb}^{-1}$ , and many analysis improvements, the most important of which are summarized below. The analyzed luminosities and references to the documentation are provided in Table I.

In order to combine the results of the six search analyses, assumptions must be made about the model to be tested. The model tested by the individual analyses' notes is a model in which Standard Model Higgs boson production proceeds, but is enhanced, in all channels, by a factor of  $R$  in the cross section. The decay branching fractions and the width of the invariant mass distribution of the Higgs boson are assumed to be those predicted by the Standard Model. Exotic models which change the Higgs boson production cross section may not follow this pattern. If a fourth generation of fermions exists, for example, it would enhance the  $gg \rightarrow H$  production cross section by a factor of roughly 9 [3], but would not enhance the  $WH$  and  $ZH$  associated production mechanisms. The Standard Model production cross sections and decay branching ratios used in this combination are the same as those used in the previous combination [1], with an update to the theoretical prediction of the  $gg \rightarrow H$  production cross section due to previously ignored two-loop electroweak contributions [4]. These corrections amount to an upwards correction of the  $gg \rightarrow H$  production cross section of up to 8% near  $m_H = 2M_W$ , and are assumed to factorize with respect to the NNLO QCD corrections already computed [5] and used in the previous combination. The cross sections used are reproduced in Table II. The cross sections listed in [5] are on a coarser mass grid than desired, and so MCFM [6] has been used to compute the remaining required cross sections, and has been found to agree well with those in [5]. The decay branching ratios are computed with HDECAY [7].

Many updates and improvements have been made to the channels since the previous combination [1], and are listed below.

- The  $WH \rightarrow \ell\nu b\bar{b}$  channels have been updated to  $2.7 \text{ fb}^{-1}$ , and several analysis improvements have been added [8]. There are nine total channels in this group, distinguished by the  $b$ -tags of the jets and the lepton category. The  $b$ -tag categories are: two tight secondary-vertex (SECVTX) [9] tags, one SECVTX tag and one Jet Probability [10] (but not SECVTX) tag, and one SECVTX tag with no tag on the other jet. The lepton categories are: triggered electron or muon candidates, isolated tracks, and forward (“Phoenix”, or PHX) electrons. Events in each lepton category are divided into the three  $b$ -tag categories. Separate neural networks are trained for each of the samples to separate the  $WH \rightarrow \ell\nu b\bar{b}$  signal from the backgrounds. The Phoenix sample is analyzed with  $1.9 \text{ fb}^{-1}$  of data [11].
- A new analysis based on boosted decision trees [12] was developed for this iteration as well. It selects events with a very high overlap with the neural network analysis described above [8], and obtains a very similar sensitivity. It was judged that neither the expected nor the observed limit would change much if the boosted decision tree analysis or the neural network analysis was included, and the neural network analysis was chosen.
- The  $WH + ZH \rightarrow \cancel{E}_T + b\bar{b}$  analysis has been updated with  $2.1 \text{ fb}^{-1}$  of data [13]. Kinematic and topological cuts have been relaxed with respect to those used in the previous analysis [14], and two neural nets are used. One is designed to remove the dominant QCD backgrounds, and the second to separate the signal from the remaining backgrounds. The data are grouped into three channels based on the tag status of the two jets. The  $b$ -tag categories are: two tight SECVTX tags, one SECVTX tag and one JetProb (but not SECVTX) tag, and one SECVTX tag with no tag on the other jet.
- The  $ZH \rightarrow \ell^+\ell^-b\bar{b}$  channels [15] have been updated to  $2.4 \text{ fb}^{-1}$  of data, and the lepton selections have been loosened. This analysis carries forwards the two-dimensional neural network approach used previously [16], with an innovative jet-energy correction technique using a neural network and assignment of the  $\cancel{E}_T$  to the jets. The selected events are grouped into two analysis channels based on the number of SECVTX tags – one or two. The discriminant variables are two neural nets designed to separate the Higgs boson signal from  $Z$ +jets and  $t\bar{t}$ , respectively, and limits are computed from two-dimensional histograms of these variables.

- The  $H \rightarrow W^+W^- \rightarrow \ell^+\nu_\ell\ell'^-\bar{\nu}_{\ell'}$  channels have been updated with  $3.0 \text{ fb}^{-1}$  [17]. Four sources of signal are considered:  $gg \rightarrow H$ ,  $WH$  associated production,  $ZH$  associated production, and vector boson fusion  $qq \rightarrow qqH$ , each assuming  $H \rightarrow W^+W^- \rightarrow \ell^+\nu_\ell\ell'^-\bar{\nu}_{\ell'}$ . In order to maximize the acceptance and separation of the signals from the SM backgrounds, dominated by nonresonant  $W^+W^-$  production, three separate analysis channels are considered: leptons+ $\cancel{E}_T$ +zero jets, one jet, or two or more jets. A combined neural network and matrix element approach is used. The mass grid for the  $H \rightarrow W^+W^- \rightarrow \ell^+\nu_\ell\ell'^-\bar{\nu}_{\ell'}$  channels has been refined to  $5 \text{ GeV}/c^2$  steps between  $m_H = 140 \text{ GeV}/c^2$  and  $180 \text{ GeV}/c^2$ , and in  $10 \text{ GeV}/c^2$  steps outside that interval. As the Tevatron combination requires a  $5 \text{ GeV}/c^2$  step everywhere, the results have been interpolated for the test mass points 100, 105, 115, 125, 135, 185 and  $195 \text{ GeV}/c^2$  by starting the signal, background and data histograms from the nearest supplied point with a test mass heavier than the one desired. The signal histograms (separately supplied for each of the four signal processes) are then scaled by the ratios of the production cross section and the decay branching ratio for  $H \rightarrow W^+W^-$ , and a separate two-loop EW correction is applied. This method is approximate because it does not interpolate the acceptance. The same interpolation scheme is applied to the  $H \rightarrow \tau^+\tau^-$  channel for the missing points at 125, 135, and  $145 \text{ GeV}/c^2$ .
- The  $WH \rightarrow WW^+W^-$  like-sign dilepton channel is included in the combination for the first time, as two independent counting experiments [18]. The “signal” region is included, as well as “Region 1”, which has a comparable signal-to-background ratio but fewer expected events. The signal predictions are computed from the acceptance, production and decay branching ratio dependences on  $m_H$  and scaled to the predicted signal given in the documentation at  $m_H = 160 \text{ GeV}/c^2$ .

## II. COMBINATION METHOD

A Bayesian technique is used to compute the observed and expected upper limits on  $R$ . The prior is flat in the product of  $R$  and the total expected signal yield after all efficiencies and acceptances are taken into account. This prior was used in the previous combination [1].

Systematic uncertainties are incorporated by marginalizing the likelihood function over variations in the uncertain parameters, called “nuisance parameters”. Each nuisance parameter is considered to be independent of the others, but each one may have an effect on any of the signal or background predictions in any of the channels. Nuisance parameters included in this combination include the integrated luminosity, the jet energy scale, the b-tag efficiency scale factor, mistag uncertainties, the lepton trigger efficiencies, the lepton identification efficiencies and fake rates, Monte Carlo generator differences, uncertainties due to missing higher-order terms in the signal and background MC predictions, Monte Carlo modeling of ISR, FSR and PDFs, background production cross sections for  $t\bar{t}$ , diboson, and other backgrounds, mistag matrix uncertainties, the heavy-flavor fraction in  $W$ +jets, and the uncertainties in non- $W$  contributions. Full listings of the nuisance parameters affecting these analyses are summarized in tables for each channel at the end of this note. The nuisance parameters affect the predicted rates of different signal and background processes, and some nuisance parameters have shape uncertainties associated with them as well.

Because the space spanned by the nuisance parameters has a very large dimension, the marginalization is done by Monte Carlo integration. Points within the nuisance parameter space are selected randomly using truncated Gaussian distributions with unit width (before truncation). The domain of each nuisance parameter is truncated in order to keep the prediction of the rate of each template non-negative; no other truncation is applied.

Rate uncertainties on template histograms are incorporated by multiplying the dependences of each rate on each nuisance parameter.

$$s_{\text{varied}} = s_{\text{central}} \prod_{i=1}^{n_{\text{params}}} (1 + f_i \eta_i) \quad (1)$$

where  $s_{\text{varied}}$  is the systematically varied normalization scale factor on a particular prediction histogram (signal or background) in a channel,  $s_{\text{central}}$  is the central-value normalization scale factor for that template,  $f_i$  is the relative uncertainty on  $s$  due to nuisance parameter  $i$ , and  $\eta_i$  is the random truncated-Gaussian-distributed nuisance parameter. Indices for the analysis channel and background or signal source template have been suppressed. The multiplicative technique used here means that the nuisance parameter truncations are all independent of each other.

Shape uncertainties are handled by varying the template shapes according to the nuisance parameters  $\eta_i$ . Systematically-varied shapes are supplied by the analysis teams as histograms which are generated with systematically varied parameters. These parameters may be the same ones as are responsible for the rate variations, and the variations are taken to be correlated. For example, a jet energy scale variation affects both the rate and the shape of most expected signal histograms. All analyses now use histograms of sophisticated multivariate discriminants in order

to present their results, and the left-right template shifting interpolation is no longer used to incorporate shape uncertainties. Instead, the simpler method of linearly interpolating between the central value shapes and the systematically varied shapes in each bin according to the value of the nuisance parameter. Shape systematics are compounded by adding linearly the changes due to several shape variations in each bin. Shape systematics are extrapolated beyond the usual  $\pm 1\sigma$  variations provided by the analysis teams. If a particular choice of shape variations results in a negative prediction for any signal or background component in any bin, then the prediction for that component is set to zero in that bin, but it does not prevent that variation from being applied to other bins. It is recommended that in the future analyzers investigate what multi-sigma variations in systematic parameters do to the predicted final discriminant shapes.

Another source of rate and shape variation is limited MC statistics in each bin of the template histograms. Each analysis supplies histograms along with their independent uncertainties in ROOT histogram objects. These uncertainties do not include the correlated rate and shape uncertainties described above, but are meant to cover the effects of MC statistics (or data statistics, if data control regions are used to predict the composition of the selected events in the signal region).

All limits are quoted at the 95% confidence level. The space of nuisance parameters is sampled with one million points in the Bayesian limit program. Expected limits are quoted as the median limit expected in a sample (2000) of background-only pseudoexperiments, and the  $\pm 1, 2\sigma$  variations. On each pseudoexperiment, new values of the nuisance parameters are drawn from the Gaussian distributions specified in the systematic uncertainty tables, and Poisson random pseudodata are drawn from the systematically smeared predictions. In order to reduce the amount of CPU used in the combination and to get more reliable  $\pm 2\sigma$  expected limit estimations, the distribution of limits in the pseudoexperiments is fit to the density function  $d(R)$ :

$$d(R) = p_1(R - p_2)^{p_3} e^{-p_4 R}, \quad (2)$$

where  $p_1$ ,  $p_2$ ,  $p_3$ , and  $p_4$  are freely-floating fit parameters. This function is then integrated to obtain the desired quantiles, which correspond to 2.275 outcomes, 16% being below the  $-1\sigma$  limit expectation, 50% being below the median expectation, 84% being below the  $+1\sigma$  expectation, and 97.725% being below the  $+2\sigma$  expectation.

### III. INDIVIDUAL CHANNEL LIMITS

In order to validate the input histogram preparation and the combination method, the observed and expected limits have been recomputed for each of the contributing channels before the final combination is performed. The rates and systematic uncertainties of each of the signal contributions and the backgrounds are compared with the available documentation. For the individual channel limits, 50000 Monte Carlo samples are performed for the observed limit, and only 25 pseudoexperiments were run for the expected limits. Tables at the end of this note compare the observed and expected limits approved by the analysis teams and the reproductions computed here. In most cases, the agreement is exquisite, since the same programs are used to compute the individual limits as is used to combine many channels together. The limits for the  $H \rightarrow W^+W^- \rightarrow \ell^+\nu_\ell\ell'^-\bar{\nu}_{\ell'}$  channels, shown in Table XVI, differ slightly from those listed in [17] as an analysis improvement was made after ICHEP 2008. The combination shown here is based on the ICHEP 2008 results [19], and thus the channel comparison is made with those results.

### IV. COMBINATION RESULTS

The results of the combination are given in Table XVIII, and in Figure 1. Figure 2 compares the observed and expected limits obtained in combination with those of the individual analyses. The same procedure for computing the individual channel limits is applied, but a joint likelihood is formed for all channels together, and variations of shared nuisance parameters, which affect both rates and shapes, are all performed with 100% correlations between parameters with the same name, and 0% correlation between parameters with different names.

The posterior of the combined results is shown in Figures 3 and 4 for each value of  $m_H$  between 100 and 200 GeV/ $c^2$  in 5 GeV/ $c^2$  steps. The distributions of the limits expected in background-only pseudoexperiments are shown in Figures 5 through 8.

To visualize the combined results better, the data are collected from all channels and are classified by the signal-to-background ratio in each bin. Bins of nearby  $s/b$  are collected together, and plotted vs  $\log_{10}(s/b)$  in Figures 9 for  $m_H = 115$  and  $160$  GeV/ $c^2$ . The data are then integrated from the high  $s/b$  side towards the lower, and the data counts are shown in Figure 10 for the same two Higgs boson masses. These integrals answer the question of how many events were observed, compared with the signal and background predictions. Because many bins of different  $s/b$  are

used to make the final limit, there is an arbitrary choice of where to put a cut to answer that question. Figure 10 shows that answer for several high- $s/b$  cuts. A drawback of this representation are that systematic uncertainties are not shown.

## V. PROJECTIONS

As data are accumulated, the sensitivity of the searches is expected to increase. A naive extrapolation of the sensitivity is to scale the median expected limit with  $1/\sqrt{\int Ldt}$ . This approximation makes several assumptions: 1) that the background levels in the high  $s/b$  bins is sufficiently large that the distribution of data events is expected to be in the Gaussian regime of the Poisson distribution, 2) that the systematic uncertainties scale with  $1/\sqrt{\int Ldt}$  for each channel, 3) that the analysis techniques remain constant, 4) that the detector performance remains constant and also does not degrade with increased instantaneous luminosity, and 5) that the tested models do not change. The experience on CDF is that the detector performance remains nearly constant, with only a mild drop due to the increased instantaneous luminosity. Larger control samples allow better constraints on systematic uncertainties, and also can be used to test extrapolations into signal regions by refining the definitions of the control samples. Analysis improvements such as increasing acceptance by exploiting previously unused trigger paths and event topologies, as well as improved separation of signal from background through the use of multivariate techniques and combinations of multivariate techniques have brought about increases in sensitivity that surpass what is expected from the  $1/\sqrt{\int Ldt}$  dependence alone. The comparison of the actual expected limits and the  $1/\sqrt{\int Ldt}$  extrapolations is shown in Figure 11 for  $m_H = 115$  and  $160$  GeV/ $c^2$ .

In Figure 11, the integrated luminosity at which to place a point is a simple unweighted average of the contributing analyses' integrated luminosities. For the  $m_H = 115$  GeV/ $c^2$  point, the the  $WH \rightarrow \ell\nu b\bar{b}$ , the  $WH + ZH \rightarrow \cancel{E}_T + b\bar{b}$ , the  $ZH \rightarrow \ell^+\ell^-b\bar{b}$ , and the  $H \rightarrow \tau^+\tau^-$  channels' luminosities are averaged, when they were available and contributed. The  $H \rightarrow \tau^+\tau^-$  channel did not exist before Winter 2008. For the  $m_H = 160$  GeV/ $c^2$  points, only the  $H \rightarrow W^+W^- \rightarrow \ell^+\nu_\ell\ell'^-\bar{\nu}_{\ell'}$  luminosity is used. In the  $m_H = 160$  GeV/ $c^2$  plot, the limits from Summer 2004 and Summer 2005 have been scaled to use the NNLO  $gg \rightarrow H$  cross section which is approximately 50% larger than the NLO cross section, which was used in the original analyses. Only the ICHEP 2008 point includes the scaling using the new 2-loop electroweak diagrams, however.

The projection figures include estimations of how much the sensitivity could be improved over time as work is done on the analyses. The estimations were made in late 2007, based on the Summer 2007 estimations of sensitivity. A factor of 1.5 in the expected limit was estimated to be attainable with improvements known to exist but not yet in the analyses, and a further factor of 1.5 was estimated from ideas that had yet to be tried. Both of these curves are shown, as the top and bottom edges of yellow bands in the figures. For the  $H \rightarrow W^+W^- \rightarrow \ell^+\nu_\ell\ell'^-\bar{\nu}_{\ell'}$  channels, the first factor of 1.5 has already been achieved.

## VI. ACKNOWLEDGEMENTS

We thank the Fermilab staff and the technical staffs of the participating institutions for their vital contributions. This work was supported by the U.S. Department of Energy and National Science Foundation; the Italian Istituto Nazionale di Fisica Nucleare; the Ministry of Education, Culture, Sports, Science and Technology of Japan; the Natural Sciences and Engineering Research Council of Canada; the National Science Council of the Republic of China; the Swiss National Science Foundation; the A.P. Sloan Foundation; the Bundesministerium für Bildung und Forschung, Germany; the Korean Science and Engineering Foundation and the Korean Research Foundation; the Science and Technology Facilities Council and the Royal Society, UK; the Institut National de Physique Nucleaire et Physique des Particules/CNRS; the Russian Foundation for Basic Research; the Ministerio de Ciencia e Innovación, Spain; the Slovak R&D Agency; and the Academy of Finland.

---

[1] CDF Collaboration, CDF Note 9282 (2008).

[2] CDF Collaboration, CDF Note 9248 (2008).

[3] E. Arik, O. Cakir, S. A. Cetin and S. Sultansoy, Acta Phys. Polon. **B37**:2839-2850 (2006). Available online as arXiv:hep-ph/0502050.

- [4] U. Aglietti, R. Bonciani, G. Degrossi, A. Vicini, “Two-loop electroweak corrections to Higgs production in proton-proton collisions”, arXiv:hep-ph/0610033v1 (2006).
- [5] TeV4LHC Higgs working group at <http://maltoni.ome.cern.ch/maltoni/TeV4LHC/SM.html>.
- [6] J.M. Campbell, R.K. Ellis, Phys. Rev. D **62**:114012 (2000), hep-ph/0006304. See also <http://mcfm.fnal.gov/index.tml>.
- [7] A. Djouadi, K.Kalinowski and M. Spira, Comp. Phys. Commun. **108C** 56 (1998).
- [8] CDF Collaboration, CDF Note 9468 (2008).
- [9] T. Aaltonen *et al.*, Phys. Rev. Lett **100** 041801 (2008);  
A. Abulencia *et al.*, Phys. Rev. D **71**, 072005 (2005).
- [10] D. Buskulic *et al.* (ALEPH Collaboration), Phys. Lett. B **313**, 535 (1993);  
F. Abe *et al.* (CDF Collaboration), Phys. Rev. D **53**, 1051 (1996);  
A. Affolder *et al.* (CDF Collaboration), Phys. Rev. D **64**, 032002 (2001), Erratum-ibid: Phys. Rev. D **67**, 119901 (2003).
- [11] CDF Collaboration, CDF Note 9219 (2008).
- [12] CDF Collaboration, CDF Note 9463 (2008).
- [13] CDF Collaboration, CDF Note 9483 (2008).
- [14] CDF Collaboration, CDF Note 8973 (2007).
- [15] CDF Collaboration, CDF Note 9475 (2008).
- [16] CDF Collaboration, CDF Note 8742 (2007).
- [17] CDF Collaboration, CDF Note 9500 (2008).
- [18] CDF Collaboration, CDF Note 7307 (2008).
- [19] M. Kirby, Presentation given at ICHEP 2008 on behalf of the CDF and D0 Collaborations, July 29-August 5, 2008, Philadelphia, PA.

TABLE I: Analyzed integrated luminosities and references for the four main CDF SM Higgs search channels combined in this note

Channel	$\int \mathcal{L} dt$ (fb $^{-1}$ )	Reference
$WH \rightarrow \ell\nu b\bar{b}$ (triggered leptons+isotrks)	2.7	[8]
$WH \rightarrow \ell\nu b\bar{b}$ (PHX)	1.9	[11]
$ZH \rightarrow \nu\bar{\nu} b\bar{b}$	2.1	[13]
$ZH \rightarrow \ell^+\ell^- b\bar{b}$	2.4	[15]
$H \rightarrow \tau^+\tau^-$	2.0	[2]
$H \rightarrow W^+W^- \rightarrow \ell^+\nu_\ell\ell'^-\bar{\nu}_{\ell'}$	3.0	[17]
$WH \rightarrow WW^+W^-$	1.9	[18]

TABLE II: The (N)NLO production cross sections and decay branching fractions for the SM Higgs boson assumed for the combination

$m_H$ (GeV/ $c^2$ )	$\sigma_{gg\rightarrow H}$ (fb)	$\sigma_{WH}$ (fb)	$\sigma_{ZH}$ (fb)	$\sigma_{VBF}$ (fb)	$B(H \rightarrow b\bar{b})$ (%)	$B(H \rightarrow \tau^+\tau^-)$ (%)	$B(H \rightarrow W^+W^-)$ (%)
100	1689.9	298.06	168.51	99.5	81.21	7.924	1.009
105	1497.1	253.37	144.57	93.3	79.57	7.838	2.216
110	1332.0	216.36	124.58	87.1	77.02	7.656	4.411
115	1188.1	185.5	107.78	79.07	73.22	7.340	7.974
120	1057.5	159.56	93.53	71.65	67.89	6.861	13.20
125	945.4	137.68	81.39	67.37	60.97	6.210	20.18
130	847.8	119.28	71.09	62.5	52.71	5.408	28.69
135	762.0	103.53	62.22	57.65	43.62	4.507	38.28
140	687.5	90.24	54.68	52.59	34.36	3.574	48.33
145	621.3	78.78	48.11	49.15	25.56	2.676	58.33
150	563.4	68.9	42.4	45.67	17.57	1.851	68.17
155	511.5	60.47	37.51	42.19	10.49	1.112	78.23
160	460.7	53.16	33.22	38.59	4.00	0.426	90.11
165	409.3			36.09	1.265	0.136	96.10
170	367.6			33.58	0.846	0.091	96.53
175	333.4			31.11	0.663	0.072	95.94
180	303.1			28.57	0.541	0.059	93.45
185	273.6			26.81	0.420	0.046	83.79
190	247.8			24.88	0.342	0.038	77.61
195	226.1			23	0.295	0.033	74.95
200	207.3			21.19	0.260	0.029	73.47

TABLE III: Systematic uncertainties for the  $WH \rightarrow \ell\nu b\bar{b}$  analysis, for the double-SECVTX tag channel and the SECVTX+JP channel. Systematic uncertainties are listed by name, see the original references for a detailed explanation of their meaning and on how they are derived. Systematic uncertainties for the  $WH$  signal shown in this table are obtained for  $m_H = 115 \text{ GeV}/c^2$ . Uncertainties are relative, in percent and are symmetric unless otherwise indicated.

SECVTX+JP  $WH \rightarrow \ell\nu b\bar{b}$   
analysis.

Contribution	W+HF	Mistags	Top	Diboson	Non-W	WH
Luminosity ( $\sigma_{\text{inel}}(p\bar{p})$ )	0	0	4	4	0	4
Luminosity Monitor	0	0	5	5	0	5
Lepton ID	0	0	2	2	0	2
Jet Energy Scale	0	0	0	0	0	3
Mistag Rate	0	8	0	0	0	0
B-Tag Efficiency	0	0	0	0	0	8
$t\bar{t}$ Cross Section	0	0	15	0	0	0
Diboson Rate	0	0	0	10	0	0
NNLO Cross Section	0	0	0	0	0	1
HF Fraction in W+jets	42	0	0	0	0	0
ISR+FSR+PDF	0	0	0	0	0	5
QCD Rate	0	0	0	0	18	0

Double-SECVTX Tagged  $WH \rightarrow \ell\nu b\bar{b}$   
analysis.

Contribution	W+HF	Mistags	Top	Diboson	Non-W	WH
Luminosity ( $\sigma_{\text{inel}}(p\bar{p})$ )	0	0	4	4	0	4
Luminosity Monitor	0	0	5	5	0	5
Lepton ID	0	0	2	2	0	2
Jet Energy Scale	0	0	0	0	0	3
Mistag Rate	0	9	0	0	0	0
B-Tag Efficiency	0	0	0	0	0	9
$t\bar{t}$ Cross Section	0	0	15	0	0	0
Diboson Rate	0	0	0	10	0	0
NNLO Cross Section	0	0	0	0	0	1
HF Fraction in W+jets	42	0	0	0	0	0
ISR+FSR+PDF	0	0	0	0	0	6
QCD Rate	0	0	0	0	18	0

TABLE IV: Observed and expected limits for the nine total  $WH \rightarrow \ell\nu b\bar{b}$  channels: (double tag + SECVTX+JP, + single SECVTX)  $\times$  (single-tag and double-tag analyses combined). The observed and median expected limits in the background-only hypothesis are listed. Also listed are the limits from [8]. The limits are all given in units of  $R = \sigma/\sigma_{SM}$ , assuming SM branching fractions.

$m_H$ (GeV/ $c^2$ )	Observed limit/SM	median expected	CDF 9468 observed	CDF 9468 expected
105	3.35	4.71	3.72	4.61
110	3.44	5.00	3.51	4.98
115	4.81	5.92	4.98	5.77
120	5.44	7.01	5.69	6.92
125	8.32	8.24	8.73	8.24
130	9.33	9.97	9.29	10.0
135	13.5	14.1	14.9	13.8
140	24.6	19.5	25.2	19.4
145	36.0	28.6	34.8	28.9
150	67.2	44.5	62.9	43.2

TABLE V: Observed and expected limits for the four  $WH \rightarrow \ell\nu b\bar{b}$  BDT channels: (1-tag + 2-tags) $\times$ (triggered leptons+loose muons). These channels are not included in the combination at this point as they have a high overlap with the  $WH \rightarrow \ell\nu b\bar{b}$  NN channels, but it is not expected to change the observed or expected combined limits much to combine either of these choices, since the performance of the BDT and NN channels is similar. The limits are all given in units of  $R = \sigma/\sigma_{SM}$ , assuming SM branching fractions.

$m_H$ (GeV/ $c^2$ )	Observed limit/SM	median expected	CDF 9463 observed	CDF 9463 expected
105	4.15	4.24	4.19	4.28
110	6.79	4.84	6.67	4.82
115	6.02	5.61	5.75	5.64
120	7.92	6.91	7.98	7.02
125	8.38	8.21	8.36	8.32
130	11.8	10.5	11.7	10.7
135	21.1	14.9	20.5	14.2
140	26.0	20.6	26.1	20.8
145	55.0	29.6	54.5	29.4

TABLE VI: Systematic uncertainties  $WH + ZH \rightarrow \cancel{E}_T + bb$ , Double-SECVTX Channel. Systematic uncertainties are listed by name, see the original references for a detailed explanation of their meaning and on how they are derived. Systematic uncertainties for  $ZH$  and  $WH$  shown in this table are obtained for  $m_H = 120$  GeV/ $c^2$ . Uncertainties are relative, in percent and are symmetric unless otherwise indicated.

	ZH	WH	Multijet	Top Pair	S. Top	Di-boson	W + h.f.	Z + h.f.
<i>Correlated uncertainties</i>								
Lumi( $\sigma_{inel}(p\bar{p})$ )	4.0%	4.0%		4.0%	4.0%	4.0%	4.0%	4.0%
Lumi Monitor	5.0%	5.0%		5.0%	5.0%	5.0%	5.0%	5.0%
Tagging SF	8.2%	8.2%		8.2%	8.2%	8.2%	8.2%	8.2%
Trigger Eff. (shape)	1.0%	1.2%		0.7%	1.1%	1.6%	1.7%	1.3%
Lepton Veto	2.0%	2.0%		2.0%	2.0%	2.0%	2.0%	2.0%
PDF Acceptance	2.0%	2.0%		2.0%	2.0%	2.0%	2.0%	2.0%
JES (shape)	+3.0% -3.0%	+3.5% -4.7%		+5.0% -6.7%	+3.0% -4.5%	+7.1% -7.3%	+7.0% -11.9%	+5.6% -9.0%
ISR		+4.4% +3.7%						
FSR		+1.8% +4.4%						
<i>Uncorrelated uncertainties</i>								
Cross-Section				6.2%	15.9%	11.5%	40%	40%
Multijet Norm. (shape)			20.6%					

TABLE VII: Systematic uncertainties  $WH + ZH \rightarrow \cancel{E}_T + bb$ , SECVTX+JP Channel. Systematic uncertainties are listed by name, see the original references for a detailed explanation of their meaning and on how they are derived. Systematic uncertainties for  $ZH$  and  $WH$  shown in this table are obtained for  $m_H = 120$  GeV/ $c^2$ . Uncertainties are relative, in percent and are symmetric unless otherwise indicated.

	ZH	WH	Multijet	Top Pair	S. Top	Di-boson	W + h.f.	Z + h.f.
<i>Correlated uncertainties</i>								
Lumi( $\sigma_{inel}(p\bar{p})$ )	4.0%	4.0%		4.0%	4.0%	4.0%	4.0%	4.0%
Lumi Monitor	5.0%	5.0%		5.0%	5.0%	5.0%	5.0%	5.0%
Tagging SF	10.9%	10.9%		10.9%	10.9%	10.9%	10.9%	10.9%
Trigger Eff. (shape)	1.2%	1.3%		0.7%	1.2%	1.2%	1.8%	1.3%
Lepton Veto	2.0%	2.0%		2.0%	2.0%	2.0%	2.0%	2.0%
PDF Acceptance	2.0%	2.0%		2.0%	2.0%	2.0%	2.0%	2.0%
JES (shape)	+3.7% -3.7%	+4.0% -4.0%		+5.5% -6.2%	+4.4% -4.6%	+6.7% -6.9%	+8.5% -6.4%	+4.8% -6.8%
ISR		+1.4% -2.9%						
FSR		+5.3% +2.5%						
<i>Uncorrelated uncertainties</i>								
Cross-Section				6.2%	15.9%	11.5%	40%	40%
Multijet Norm. (shape)			15.6%					



TABLE X: Observed and expected limits for the  $ZH \rightarrow \ell^+ \ell^- b \bar{b}$  channels, with the single-tag and double-tag analyses combined. The observed and median expected limits are listed. Also listed are the limits from [15]. The limits are all given in units of  $R = \sigma/\sigma_{SM}$ , assuming SM branching fractions.

$m_H$ (GeV/ $c^2$ )	Observed limit/SM	median expected	CDF 9475 observed	CDF 9475 expected
105	8.02	8.33	8.02	8.15
110	10.7	10.5	10.62	10.7
115	11.7	11.5	11.57	11.79
120	13.1	14.4	13.36	14.51
125	17.5	17.3	17.16	16.67
130	21.1	21.3	21.23	21.58
135	26.6	29.7	27.11	29.38
140	40.7	41.5	39.73	42.04
145	63.3	69.3	65.01	64.36

TABLE XI: Systematic uncertainties on the contributions for the  $H \rightarrow \tau^+ \tau^-$  channel. Systematic uncertainties are listed by name, see the original references for a detailed explanation of their meaning and on how they are derived. Uncertainties with provided shape systematics are labeled with “s”. Systematic uncertainties for  $H$  shown in this table are obtained for  $m_H = 115$  GeV/ $c^2$ . Uncertainties are relative, in percent and are symmetric unless otherwise indicated. The systematic uncertainty called “Normalization” includes effects of the inelastic  $p\bar{p}$  cross section, the luminosity monitor acceptance, and the lepton trigger acceptance. It is considered to be entirely correlated with the luminosity uncertainty.

Contribution	$Z/\gamma^* \rightarrow \tau\tau$	$Z/\gamma^* \rightarrow \ell\ell$	$t\bar{t}$	diboson	jet $\rightarrow \tau$	W+jet	WH	ZH	VBF	H
Luminosity	6	6	6	6	-	-	6	6	6	6
$e, \mu$ Trigger	1	1	1	1	-	-	1	1	1	1
$\tau$ Trigger	3	3	3	3	-	-	3	3	3	3
$e, \mu, \tau$ ID	3	3	3	3	-	-	3	3	3	3
PDF Uncertainty	1	1	1	1	-	-	1	1	1	1
ISR/FSR	-	-	-	-	-	-	2/0	1/1	3/1	12/1
JES (shape)	16	13	2	10	-	-	3	3	4	14
Cross Section or Norm.	2	2	13	10	-	15	5	5	10	10
MC model	20	10	-	-	-	-	-	-	-	-

TABLE XII: Observed and expected limits for the  $H \rightarrow \tau^+ \tau^-$  channel. The observed and median expected limits are listed. Also listed are the limits from [2]. The limits are all given in units of  $R = \sigma/\sigma_{SM}$ , assuming SM branching fractions.

$m_H$ (GeV/ $c^2$ )	Observed limit/SM	median expected	CDF 9179 observed	CDF 9179 expected
110	30.1	25.5	32.5	25.8
115	30.9	24.9	30.5	24.8
120	29.6	24.2	30.0	24.2
130	37.2	32.1	39.5	32.3
140	62.4	52.8	67.5	52.8
150	146.9	118.8	159.0	111.7

TABLE XIII: Systematic uncertainties on the contributions for CDF's  $H \rightarrow W^+W^- \rightarrow \ell^\pm \ell'^\mp$  channel with zero jets. Systematic uncertainties are listed by name, see the original references for a detailed explanation of their meaning and on how they are derived. Systematic uncertainties for  $gg \rightarrow H$  shown in this table are obtained for  $m_H = 160 \text{ GeV}/c^2$ . Uncertainties are relative, in percent and are symmetric unless otherwise indicated. Uncertainties in bold are correlated across jet bins but not across channels. Uncertainties in italics are correlated across jet bins and across appropriate channels.

Uncertainty Source	<i>WW</i>	<i>WZ</i>	<i>ZZ</i>	<i>tt</i>	<i>DY</i>	<i>W<math>\gamma</math></i>	<i>W+jet</i>	<i>gg <math>\rightarrow</math> H</i>	<i>WH</i>	<i>ZH</i>	<i>VBF</i>
<b>Cross Section</b>											
Scale								10.9%			
PDF Model								5.1%			
Total	<i>10.0%</i>	<i>10.0%</i>	<i>10.0%</i>	15.0%	5.0%	10.0%		12.0%			
<b>Acceptance</b>											
Scale (leptons)								2.5%			
Scale (jets)								4.6%			
PDF Model (leptons)	1.9%	2.7%	2.7%	2.1%	4.1%	2.2%		1.5%			
PDF Model (jets)								0.9%			
Higher-order Diagrams	<b>5.5%</b>	<b>10.0%</b>	<b>10.0%</b>	10.0%	<b>5.0%</b>	<b>10.0%</b>					
Missing Et Modeling	1.0%	1.0%	1.0%	1.0%	20.0%	1.0%		1.0%			
Conversion Modeling						20.0%					
Jet Fake Rates (Low S/B)							21.5%				
(High S/B)							27.7%				
MC Run Dependence	3.9%			4.5%		4.5%		3.7%			
Lepton ID Efficiencies	2.0%	1.7%	2.0%	2.0%	1.9%	1.4%		1.9%			
Trigger Efficiencies	2.1%	2.1%	2.1%	2.0%	3.4%	7.0%		3.3%			
<b>Luminosity</b>	5.9%	5.9%	5.9%	5.9%	5.9%	5.9%		5.9%			

TABLE XIV: Systematic uncertainties on the contributions for CDF's  $H \rightarrow W^+W^- \rightarrow \ell^\pm \ell'^\mp$  channel with one jet. Systematic uncertainties are listed by name, see the original references for a detailed explanation of their meaning and on how they are derived. Systematic uncertainties for  $gg \rightarrow H$  shown in this table are obtained for  $m_H = 160 \text{ GeV}/c^2$ . Uncertainties are relative, in percent and are symmetric unless otherwise indicated. Uncertainties in bold are correlated across jet bins but not across channels. Uncertainties in italics are correlated across jet bins and across appropriate channels.

Uncertainty Source	$WW$	$WZ$	$ZZ$	$tt$	$DY$	$W\gamma$	$W+\text{jet}$	$gg \rightarrow H$	$WH$	$ZH$	VBF
<b>Cross Section</b>											
Scale								10.9%			
PDF Model								5.1%			
Total	<i>10.0%</i>	<i>10.0%</i>	<i>10.0%</i>	15.0%	5.0%	10.0%		12.0%	5.0%	5.0%	10.0%
<b>Acceptance</b>											
Scale (leptons)								2.8%			
Scale (jets)								-5.1%			
PDF Model (leptons)	1.9%	2.7%	2.7%	2.1%	4.1%	2.2%		1.7%	1.2%	0.9%	2.2%
PDF Model (jets)								-1.9%			
Higher-order Diagrams	<b>5.5%</b>	<b>10.0%</b>	<b>10.0%</b>	10.0%	<b>5.0%</b>	<b>10.0%</b>			<i>10.0%</i>	<i>10.0%</i>	<i>10.0%</i>
Missing Et Modeling	1.0%	1.0%	1.0%	1.0%	20.0%	1.0%		1.0%	1.0%	1.0%	1.0%
Conversion Modeling						20.0%					
Jet Fake Rates											
(Low S/B)							22.2%				
(High S/B)							31.5%				
MC Run Dependence	1.8%			2.2%		2.2%		2.6%	2.6%	1.9%	2.8%
Lepton ID Efficiencies	2.0%	2.0%	2.2%	1.8%	2.0%	2.0%		1.9%	1.9%	1.9%	1.9%
Trigger Efficiencies	2.1%	2.1%	2.1%	2.0%	3.4%	7.0%		3.3%	2.1%	2.1%	3.3%
<b>Luminosity</b>	5.9%	5.9%	5.9%	5.9%	5.9%	5.9%		5.9%	5.9%	5.9%	5.9%

TABLE XV: Systematic uncertainties on the contributions for CDF's  $H \rightarrow W^+W^- \rightarrow \ell^\pm \ell'^\mp$  channel with two or more jets. Systematic uncertainties are listed by name, see the original references for a detailed explanation of their meaning and on how they are derived. Systematic uncertainties for  $gg \rightarrow H$  shown in this table are obtained for  $m_H = 160 \text{ GeV}/c^2$ . Uncertainties are relative, in percent and are symmetric unless otherwise indicated. Uncertainties in bold are correlated across jet bins but not across channels. Uncertainties in italics are correlated across jet bins and across appropriate channels.

Uncertainty Source	$WW$	$WZ$	$ZZ$	$t\bar{t}$	DY	$W\gamma$	$W+\text{jet}$	$gg \rightarrow H$	$WH$	$ZH$	VBF
<b>Cross Section</b>											
Scale								10.9%			
PDF Model								5.1%			
Total	<i>10.0%</i>	<i>10.0%</i>	<i>10.0%</i>	15.0%	5.0%	10.0%		12.0%	5.0%	5.0%	10.0%
<b>Acceptance</b>											
Scale (leptons)								3.1%			
Scale (jets)								-8.7%			
PDF Model (leptons)	1.9%	2.7%	2.7%	2.1%	4.1%	2.2%		2.0%	1.2%	0.9%	2.2%
PDF Model (jets)								-2.8%			
Higher-order Diagrams	<b>10.0%</b>	<b>10.0%</b>	<b>10.0%</b>	10.0%	<b>10.0%</b>	<b>10.0%</b>			<i>10.0%</i>	<i>10.0%</i>	<i>10.0%</i>
Missing Et Modeling	1.0%	1.0%	1.0%	1.0%	20.0%	1.0%		1.0%	1.0%	1.0%	1.0%
Conversion Modeling						20.0%					
$b$ -tag Veto				7.0%							
Jet Fake Rates							27.1%				
MC Run Dependence	1.0%			1.0%		1.0%		1.7%	2.0%	1.9%	2.6%
Lepton ID Efficiencies	1.9%	2.9%	1.9%	1.9%	1.9%	1.9%		1.9%	1.9%	1.9%	1.9%
Trigger Efficiencies	2.1%	2.1%	2.1%	2.0%	3.4%	7.0%		3.3%	2.1%	2.1%	3.3%
<b>Luminosity</b>	5.9%	5.9%	5.9%	5.9%	5.9%	5.9%		5.9%	5.9%	5.9%	5.9%

TABLE XVI: Observed and expected limits for the  $gg \rightarrow H \rightarrow W^+W^- \rightarrow \ell^+\nu_\ell\ell'^-\bar{\nu}_{\ell'}$  channel, with the high- $s/b$  and low- $s/b$  analyses combined, for all three jet categories. The observed and median expected limits are listed. Also listed are the limits from [17]. The limits are all given in units of  $R = \sigma/\sigma_{SM}$ , assuming SM branching fractions. The columns labeled ICHEP 2008 list numbers shown in [19]

$m_H$ (GeV/ $c^2$ )	Observed limit/SM	median expected	ICHEP 2008 observed	ICHEP 2008 expected
110	68.5	37.8	71.06	37.81
115	24.2	18.4		
120	17.5	12.6	15.59	12.49
125	8.61	7.86		
130	7.01	6.04	7.04	6.00
135	5.05	4.34		
140	4.69	3.86	4.38	3.83
145	3.43	3.36	3.41	3.34
150	3.42	2.77	3.27	2.78
155	2.26	2.25	2.22	2.28
160	1.59	1.68	1.54	1.68
165	1.64	1.63	1.63	1.64
170	1.83	1.93	1.74	1.87
175	1.93	2.36	2.07	2.35
180	2.51	2.78	2.62	2.77
185	4.46	3.88		
190	5.08	4.51	5.26	4.55
195	8.41	5.44		
200	9.84	5.96	10.63	6.22

TABLE XVII: Systematic uncertainties on the contributions for CDF 's  $WH \rightarrow WWW \rightarrow \ell'^{\pm}\ell'^{\pm}$  channel. Systematic uncertainties are listed by name, see the original references for a detailed explanation of their meaning and on how they are derived. Systematic uncertainties for  $WH$  shown in this table are obtained for  $m_H = 160$  GeV/ $c^2$ . Uncertainties are relative, in percent and are symmetric unless otherwise indicated. The diboson contribution to the final selected sample is negligible.

Contribution	$\gamma$ Conversions	Fakes	WH
Statistical Uncertainty	0	0	1.6
Fake Rate	0	25	0
Conversions	25	0	0
Luminosity	0	0	6
ISR	0	0	4.0
FSR	0	0	4.1
PDF	0	0	1.9
Lepton ID	0	0	1.2

TABLE XVIII: Observed and expected limits for all CDF SM Higgs boson search channels combined. The observed and median expected limits are listed, as well as  $\pm 1, 2\sigma$  variation on the expected limits from statistical fluctuations assuming only background processes contribute. The limits are all given in units of  $R = \sigma/\sigma_{SM}$ , assuming SM branching fractions.

$m_H$ (GeV/ $c^2$ )	Observed limit/SM	$-2\sigma$ expected	$-1\sigma$ expected	median expected	$+1\sigma$ expected	$+2\sigma$ expected
100	3.01	1.43	2.07	3.13	4.78	7.10
105	2.87	1.30	1.91	2.98	4.62	6.95
110	3.34	1.47	2.15	3.29	5.00	7.35
115	4.19	1.58	2.32	3.56	5.43	8.05
120	4.53	1.93	2.75	4.15	6.29	9.31
125	6.04	1.87	2.77	4.29	6.55	9.72
130	5.62	1.99	2.80	4.21	6.38	9.46
135	5.40	1.58	2.29	3.52	5.42	8.12
140	5.45	1.48	2.20	3.41	5.23	7.79
145	3.92	1.33	2.02	3.11	4.71	6.90
150	4.13	1.12	1.65	2.60	4.08	6.20
155	2.27	1.19	1.63	2.30	3.24	4.52
160	1.52	0.86	1.17	1.68	2.43	3.50
165	1.64	0.80	1.12	1.60	2.26	3.13
170	1.80	0.98	1.33	1.90	2.73	3.88
175	1.97	1.22	1.63	2.35	3.45	5.03
180	2.52	1.35	1.89	2.74	3.95	5.60
185	4.47	1.90	2.64	3.81	5.48	7.76
190	5.47	2.15	3.11	4.54	6.50	9.09
195	9.05	2.64	3.62	5.33	7.94	11.63
200	10.18	2.92	4.15	6.19	9.22	13.44

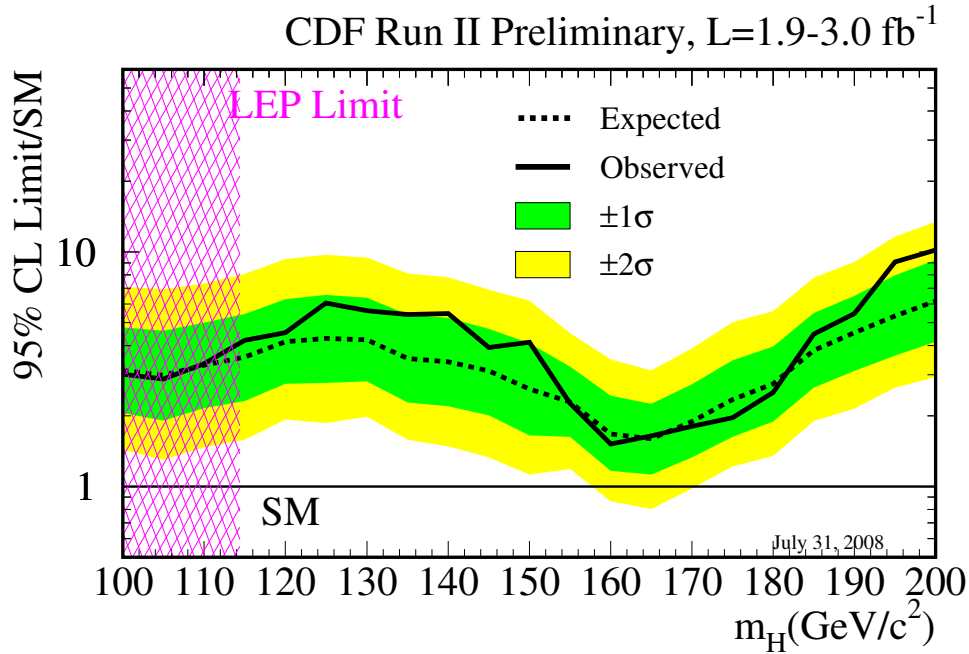


FIG. 1: The 95% CL upper limit on  $R = \sigma/\sigma_{SM}$ , shown as a function of  $m_H$ , for the combination of all of CDF's SM Higgs search channels. The  $\pm 1, 2\sigma$  bands on the expected limits are also shown, centered on the median expected limit.

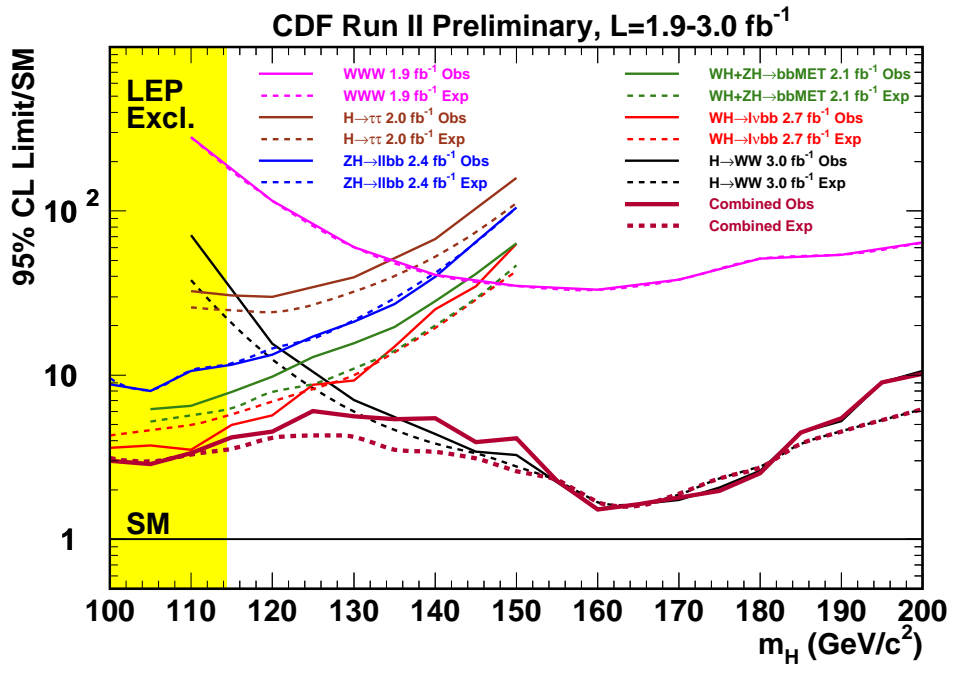


FIG. 2: The 95% CL upper limit on  $R = \sigma/\sigma_{SM}$ , shown as a function of  $m_H$ , shown separately for each analysis and for the combination. Dashed lines indicate the median expected limits, and the solid lines show the observed limits. The LEP bound  $m_H > 114.4$  GeV/ $c^2$  is shown in yellow.

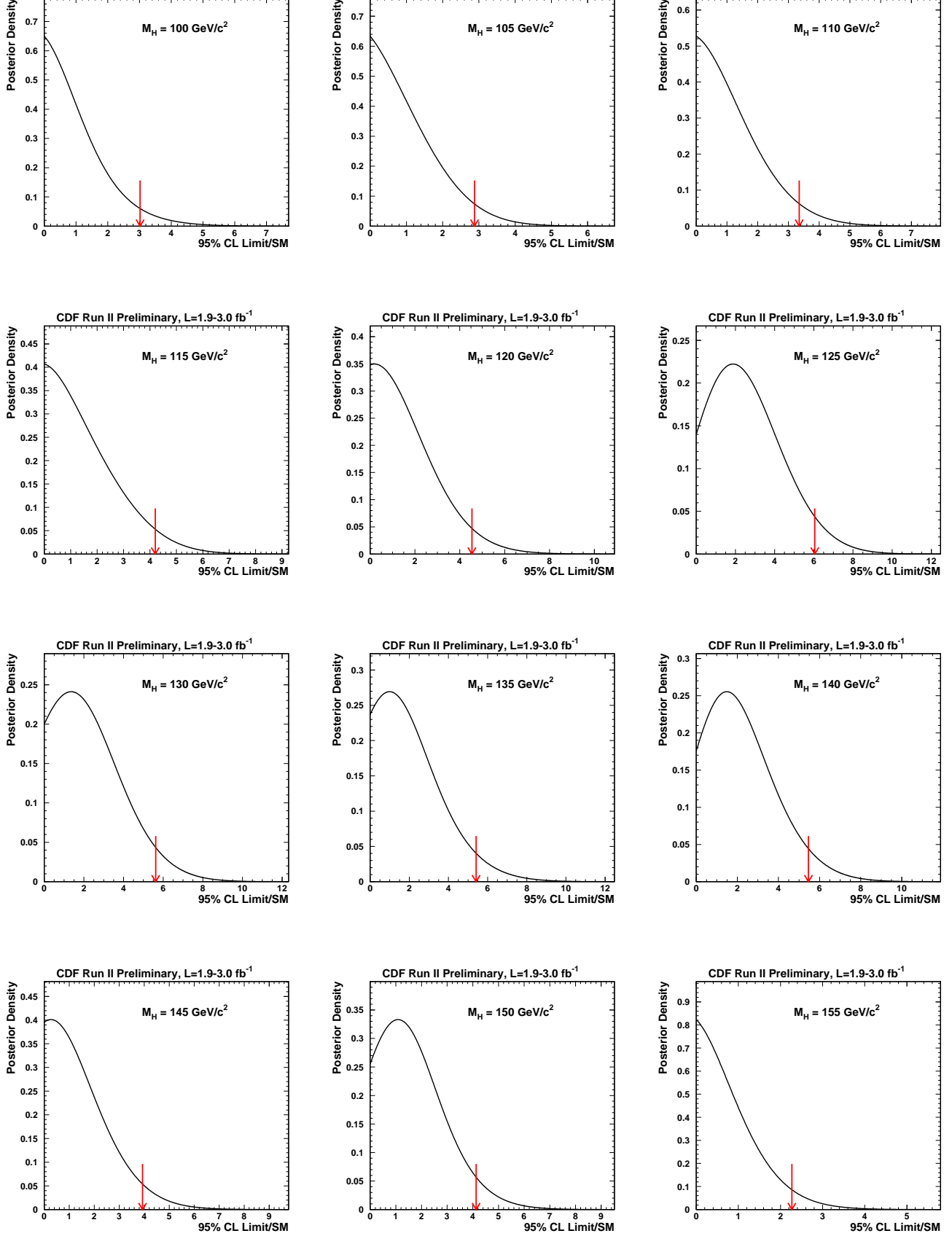


FIG. 3: The posterior densities and observed upper limits on  $R = \sigma/\sigma_{SM}$ , shown separately shown for Higgs boson masses of 100 through 155  $\text{GeV}/c^2$ .

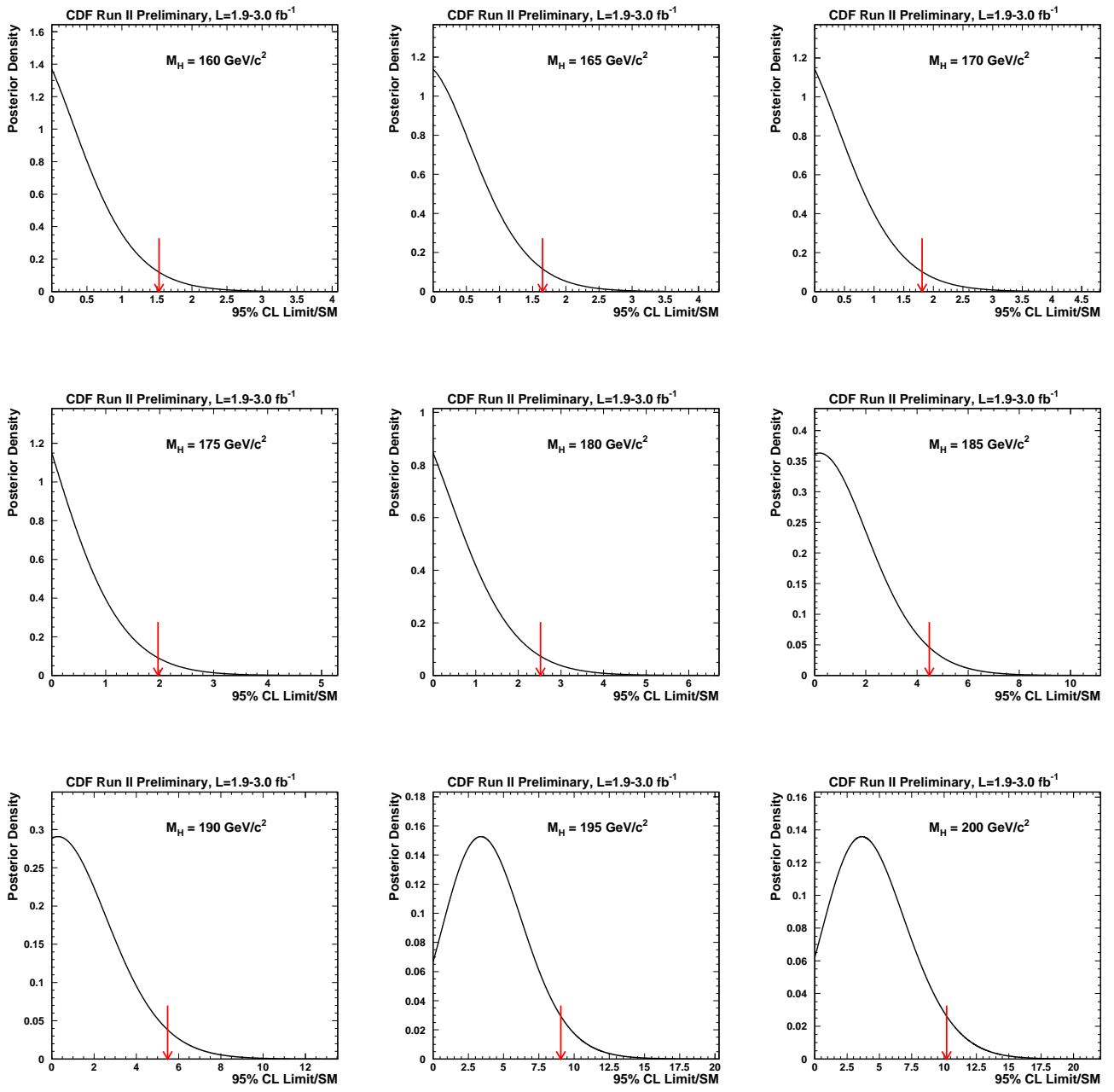


FIG. 4: The posterior densities and observed upper limits on  $R = \sigma/\sigma_{SM}$ , shown separately shown for Higgs boson masses of 160 through 200 GeV/c<sup>2</sup>.

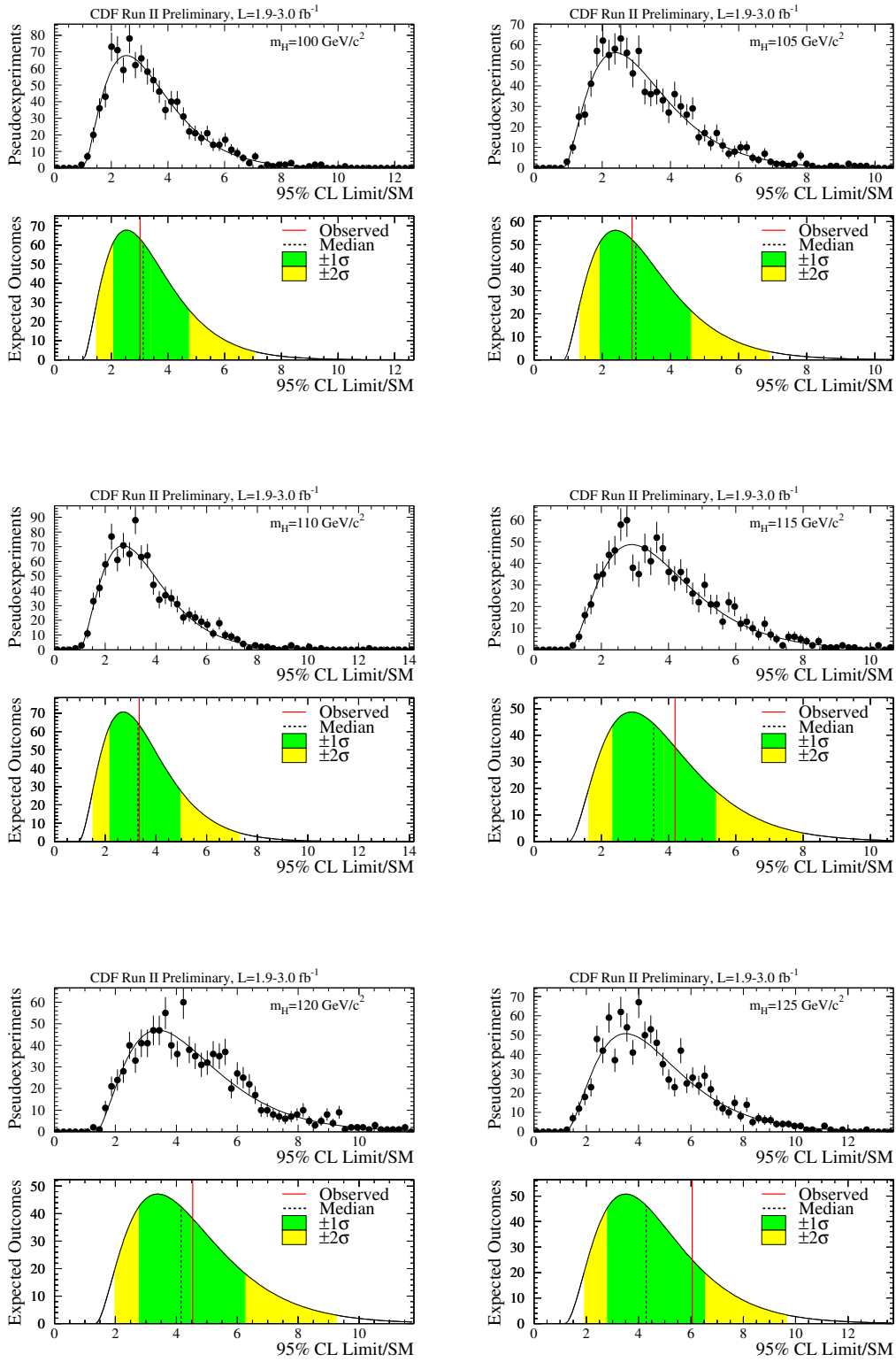


FIG. 5: The distributions of expected upper limits on  $R = \sigma/\sigma_{\text{SM}}$  assuming no signal is truly present in the data, separately shown for Higgs boson masses of 100, 105, 110, 115, 120 and 125  $\text{GeV}/c^2$ .

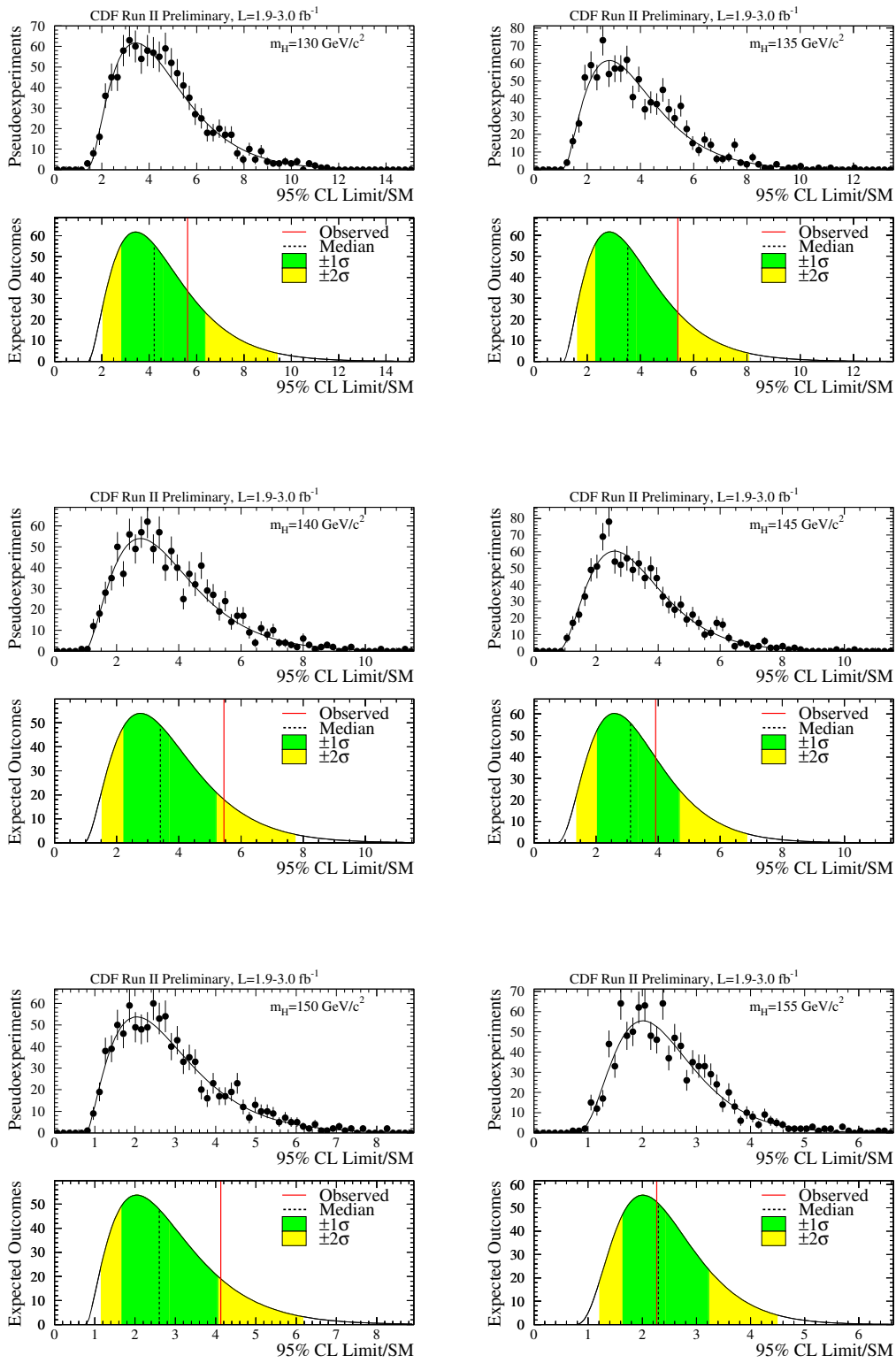


FIG. 6: The distributions of expected upper limits on  $R = \sigma/\sigma_{\text{SM}}$  assuming no signal is truly present in the data, separately shown for Higgs boson masses of 130, 135, 140, 145, 150 and 155  $\text{GeV}/c^2$ .

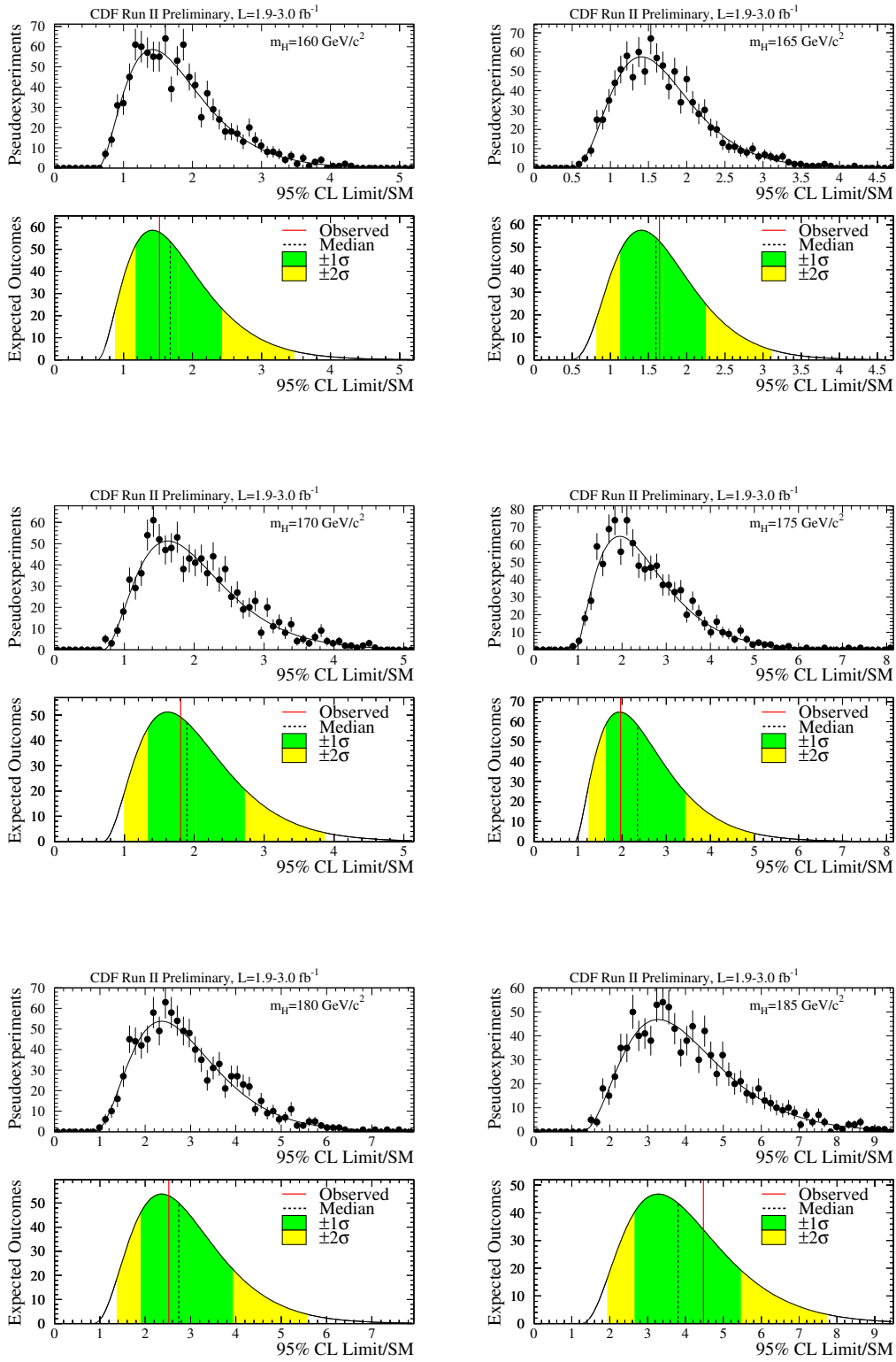


FIG. 7: The distributions of expected upper limits on  $R = \sigma/\sigma_{\text{SM}}$  assuming no signal is truly present in the data, separately shown for Higgs boson masses of 160, 165, 170, 175, 180 and 185  $\text{GeV}/c^2$ .

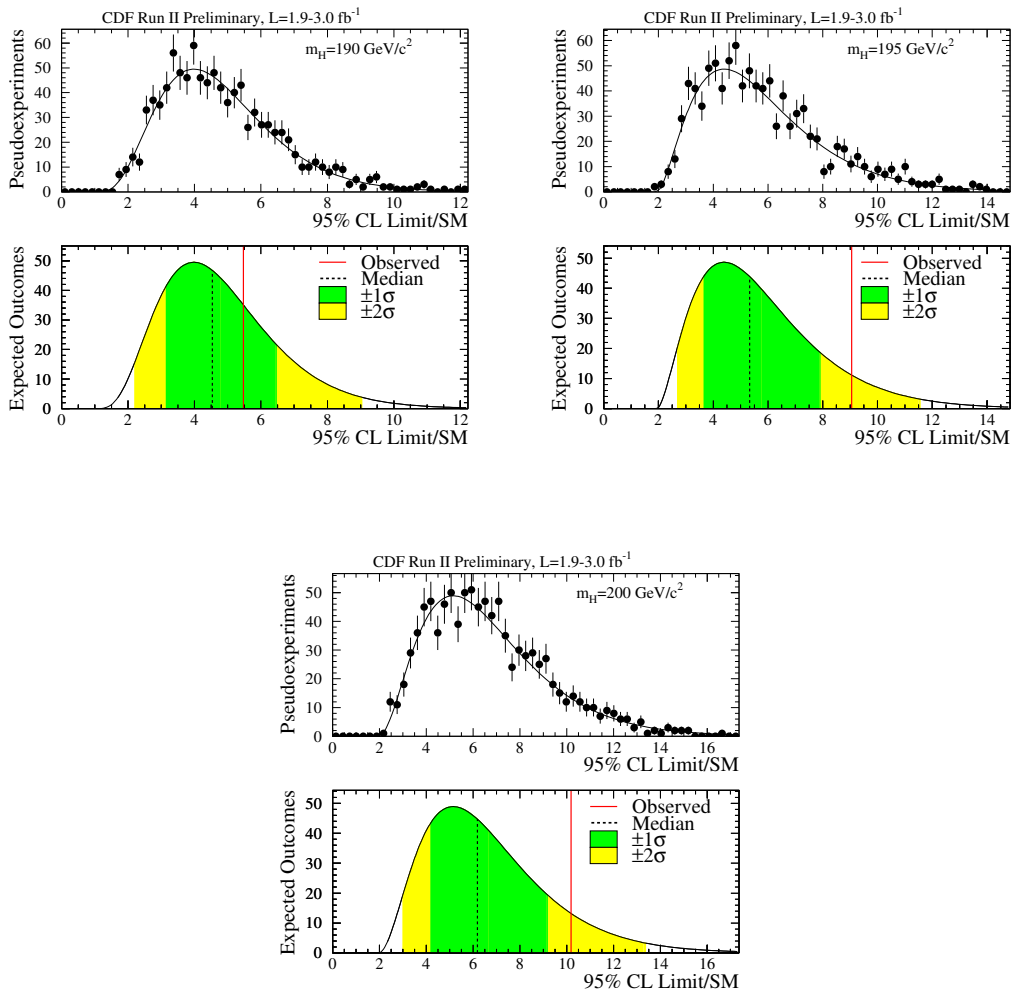


FIG. 8: The distributions of expected upper limits on  $R = \sigma/\sigma_{\text{SM}}$  assuming no signal is truly present in the data, separately shown for Higgs boson masses of 190, 195 and 200  $\text{GeV}/c^2$ .

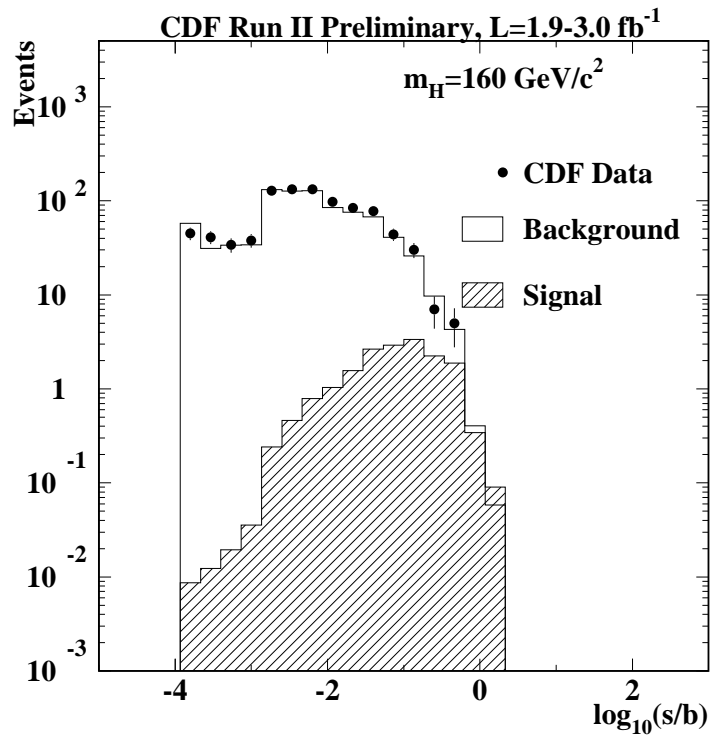
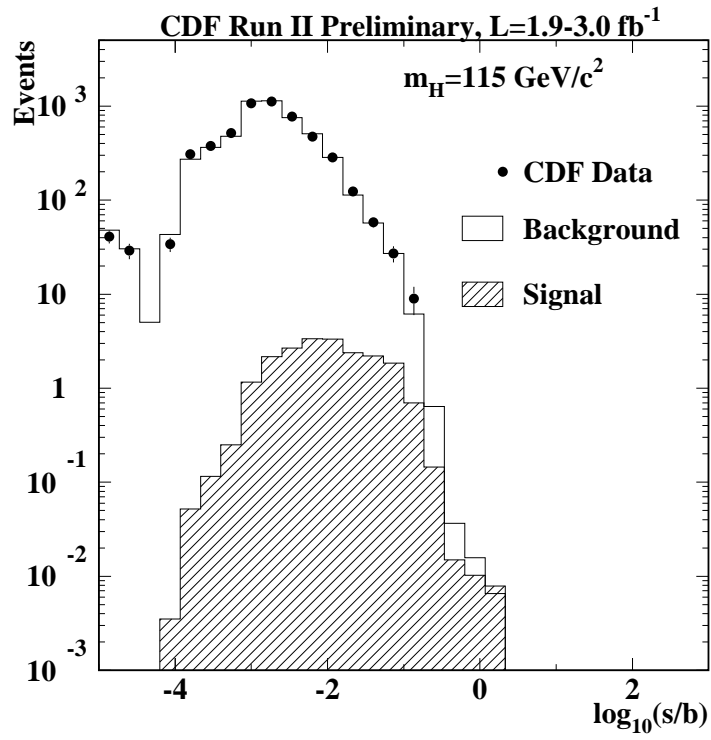


FIG. 9: Signal predictions, background predictions, and observed data, collected in bins sorted by  $s/b$ , for all channels added together. These are shown for  $m_H=115$  and  $160 \text{ GeV}/c^2$ .

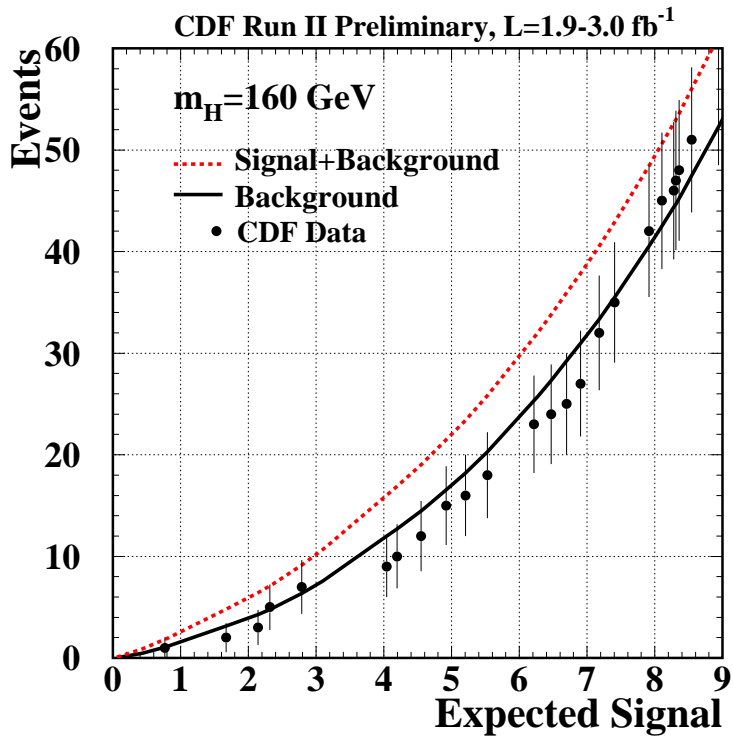
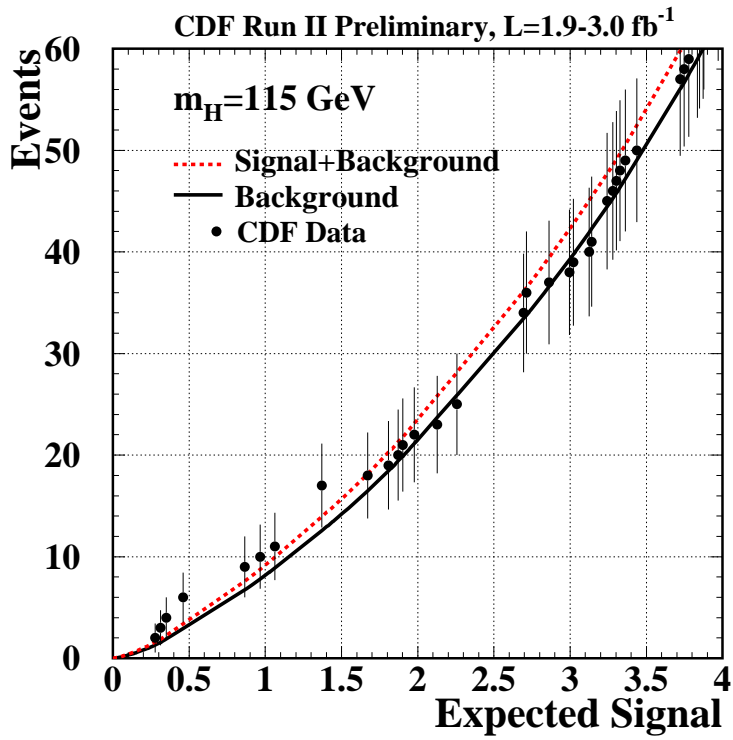
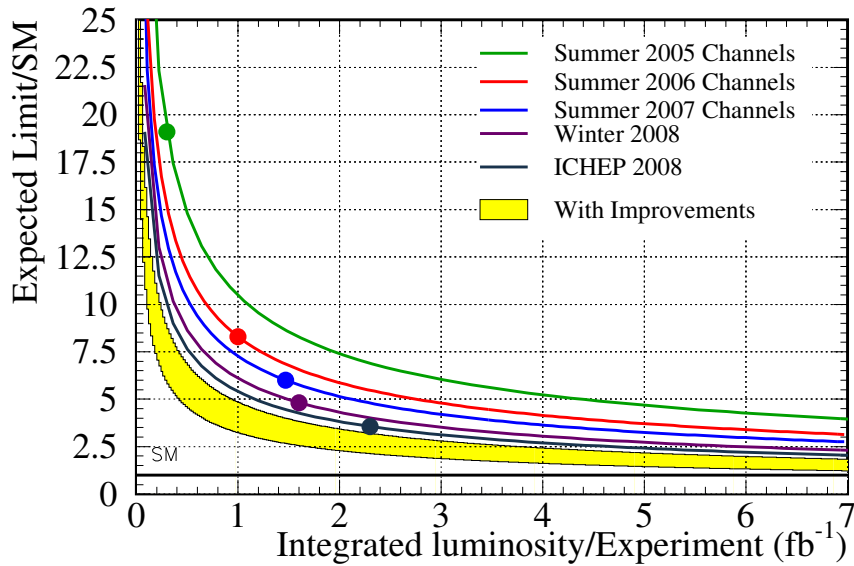


FIG. 10: Integrated signal predictions, background predictions, and observed data, collected in bins sorted by  $s/b$ , for all channels added together. These are shown for  $m_H=115$  and  $160 \text{ GeV}/c^2$ .

## CDF Run II Preliminary, $m_H=115$ GeV



## CDF Run II Preliminary, $m_H=160$ GeV

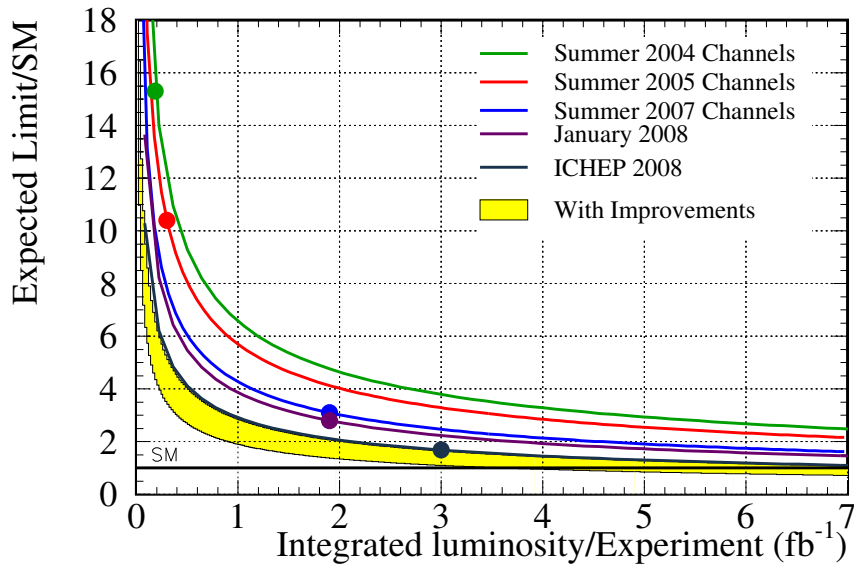


FIG. 11: Sensitivity projections and achieved sensitivities for the combined CDF Higgs boson searches, at  $m_H = 115$  and  $160 \text{ GeV}/c^2$ . The curves are proportional to  $1/\sqrt{\int L dt}$  extrapolations of the median expected limits, and each analysis update corresponds to a new point with a new curve. The yellow bands indicate ranges of possible improvements in performance, relative to the Summer 2007 sensitivity. The top of the yellow bands is a factor of 1.5 below the Summer 2007 curve, and the bottom of the yellow bands are a further factor of 1.5 below the top of the yellow bands.